1992ApJ...400..330S

THE ASTROPHYSICAL JOURNAL, 400:330–343, 1992 November 20
© 1992. The American Astronomical Society. All rights reserved. Printed in U.S.A.

# *GINGA* OBSERVATIONS OF THE DIPPING LOW-MASS X-RAY BINARIES XB 1916−053 AND EXO 0748−676

ALAN P. SMALE
USRA Research Scientist, Laboratory for High Energy Astrophysics, Code 666, NASA/Goddard Space Flight Center, Greenbelt, MD 20771
KOJI MUKAI
Center for EUV Astrophysics, University of California, 2150 Kittredge Street, Berkeley, CA 94720
O. REES WILLIAMS
Astrophysics Division (SA), ESTEC, Keplerlaan 1, Postbus 299, 2200 AG Noordwijk, The Netherlands
MARK H. JONES
Astronomy Unit, School of Mathematical Sciences, Queen Mary and Westfield College, Mile End Road, London E1 4NS
AND
ROBIN H. D. CORBET
Department of Astronomy and Astrophysics, 525 Davey Laboratory, Pennsylvania State University, University Park, PA 16802
*Received 1992 February 10; accepted 1992 May 27*

## ABSTRACT

Several low-mass X-ray binaries display pronounced dips of variable depth and duration in their X-ray light curves, due to the periodic occultation of the central source by azimuthal accretion disk structure. We present results from *Ginga* observations of two such sources, XB 1916−053 and EXO 0748−676.

XB 1916−053 was observed for 3 days in 1988 September. Periodicity studies show results consistent with those from previous *Ginga* observations (Smale et al. 1989), specifically that the derived X-ray period is shorter than the optical period by ∼1%. We discuss this problem in detail, drawing from current knowledge on CVs as well as LMXBs, and describe a more refined model for the system. If the accretion disk in XB 1916−053 is elliptical, the azimuthal position of the structure remains fixed in the binary reference frame, and thus the primary X-ray dips recur at the orbital period. However, the vertical extent of the disk structure, and thus the reprocessed optical emission, will be modulated on the beat between the orbital and disk precession periods, producing the observed period discrepancy.

Three bursts were detected during the observation of XB 1916−053, the second of which occurred during a dip. Spectral analysis suggests that the second burst caused an almost instantaneous ionization of the absorbing medium in the line of sight; this material then returned to its equilibrium state on the same time scale as the burst decay. We show that the theoretical ionization and recombination time scales are short enough for this to be feasible, and that the total burst fluence is large enough to produce such an effect. In addition, we find evidence that the bursts cause a ∼threefold increase in the emission component from the disk.

We observed EXO 0748−676 in 1989 March, also for 3 days. The source was found to be in a bright state, and data were obtained covering two eclipses and many dips. We have analyzed intensity-selected spectra accumulated from the dipping intervals of both XB 1916−053 and EXO 0748−676, and in addition have performed simulations to assess the effects of a rapidly changing column density upon the observed spectra from these sources. We show that during dipping intervals, where $N_H$ varies on a time scale shorter than the spectral integration time, spectral mixing can produce an apparent low-energy component in the data. Thus, rapidly variable simple absorption is indistinguishable from partial covering. From the variability analysis, we place loose limits upon the possible clumpiness of the material responsible for the accretion disk structure in XB 1916−053 and EXO 0748−676.

*Subject headings:* binaries: eclipsing — stars: individual (XB 1916−053, EXO 0748−676) — X-rays: stars

## 1. INTRODUCTION

There are about 10 low-mass X-ray binaries (LMXBs) that are currently known to display periodic dipping behavior in their X-ray light curves. For each individual source, these dips appear to be variable in length and duration; however, their phasing relative to X-ray eclipses and optical maximum light generally indicates that the location of the obscuring material is fixed in the rest frame of the binary. It is believed that we observe these sources at a high inclination, such that azimuthal structure on the accretion disk extends vertically above the plane of the binary and periodically blocks the line of sight to the central X-ray–producing regions.

The location of the accretion disk structure, and the mechanism by which it is formed and maintained, is still a matter for debate. According to the widely used empirical model, dips are caused by a bulge in the outer regions of the accretion disk associated with the impact point of the accretion stream. In the theoretical model of Frank, King, & Lasota (1987), however, the structures are placed at the ballistic circularization radius, where stream material flowing above and below the disk accumulates to form a ring. Lubow (1989) has shown that the stream has sufficient scale height at the disk edge for some material to flow above the disk, but that such material converges onto the orbital plane near the periastron passage of the



© American Astronomical Society • Provided by the NASA Astrophysics Data System

1992ApJ...400..330S



stream to merge into the disk. Applied to dipping LMXBs, this picture suggests that the overflowing material, particularly near the stream periastron, may cause the dips.

Although the latter picture is appealing, it can be ruled out for at least one low-mass system. The highly inclined source X1822−371 shows a narrow partial eclipse feature in its X-ray light curve due to the eclipse of an accretion disk corona by the companion star, and also a broad modulation caused by variable obscuration of this corona by disk structure similar to that discussed above. In this case, detailed modeling of both X-ray and optical light curves shows that the structure must be located on the outer rim of the accretion disk (White & Holt 1982; Mason & Córdova 1982; Hellier & Mason 1989). In addition, particle simulations by Hirose, Osaki, & Mineshige (1991) show that extended azimuthal structure on the rim of the disk can be produced and sustained as a result of the stream-disk interactions, arguing against the Frank et al. (1987) model.

XB 1916−053 (V1405 Aql) has the shortest period known (50 minutes) among the dippers, implying that the companion is hydrogen-deficient (Nelson, Rappaport, & Joss 1986). Data from three *EXOSAT* observations performed in 1983 and 1985 revealed considerable variability in the form of the light curves, ranging from a total absence of dipping activity, through intervals where a single ("primary") dip is seen per orbital cycle with a duty cycle of around 10%, to a complex mode in which two broad, irregular dips were observed in each cycle separated by roughly 180° in phase (Smale et al. 1988, hereafter Paper I). The absence of eclipses requires that for this system the inclination must be less than 79°. The first two *Ginga* observations of XB 1916−053, performed in 1987 May and September (Smale et al. 1989, hereafter Paper II) confirmed a 1% discrepancy between the optical and X-ray periodicities of the system, and showed that the appearance of the secondary dip and the breadth of both dips varied over 4 days. We report here the results of a third *Ginga* observation of XB 1916−053 and perform a detailed analysis of the spectra from the second and third observations.

EXO 0748−676 (UY Vol) displays almost total eclipses by the companion star every 3.82 hr, defining both the orbital period and the system geometry. In addition to the eclipses, dips of irregular form and duration are observed, preferentially at orbital phases $\phi = 0.65$ and 0.8–0.2 relative to the eclipse center. Using the 8 minute duration of the eclipses and assuming a main-sequence companion, Parmar et al. (1986) find a companion mass of 0.45 $M_\odot$ and a system inclination of $i = 75°$, suggesting that similar disk structures may be responsible for the dip behavior in both XB 1916−053 and EXO 0748−676. In this paper we present results from the first *Ginga* observation of EXO 0748−676.

## 2. THE *Ginga* OBSERVATIONS

The principal instrument on board *Ginga* was the LAC, consisting of eight large-area low-background proportional counters with a total effective area of 4000 cm$^2$, sensitive in the 0.5–37 keV range (Turner et al. 1989). It operated in near-Earth orbit, and the light curves therefore suffered gaps due to Earth occultation and transit through the SAA and other regions of high particle background.

The third *Ginga* observation of XB 1916−053 was carried out between 1988 September 9 10:51 UT and September 11 22:19 UT. The total duration of the observation was ~215,000 s (~2.5 days), covering 71 orbits of XB 1916−053 with a total on-source time of 80,300 s. Although a short adjacent background observation was performed, it was not of sufficient length to be useful, and did not include any intervals of high background. Therefore, a universal background model (including particle events and the radioactivity induced by SAA passages) was applied (Hayashida et al. 1989). For a source of this intensity, a background subtraction performed in this way is expected to be acceptable. The MPC1 data collection mode was used throughout, with PHA data being accumulated into 48 channels spanning 0.5–37 keV, and a time resolution of 4 to 16 s. We present the light curve from this observation in Figure 1. The small apparent changes in the quiescent (nondip, nonburst) flux level may be due to slight changes in the pointing offset.

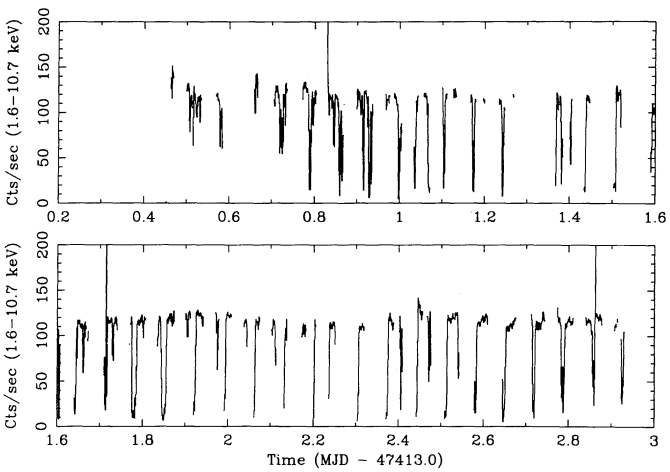


FIG. 1.—The light curve from the third *Ginga* observation of XB 1916−053 in 1988 September, summed into 64 s bins.

We observed EXO 0748−676 from 1989 March 24 17:30 UT until March 26 04:20 UT. The source was observed continuously apart from a brief break at March 25 07:20–12:30, when the *Ginga* team changed the pointing to monitor three transient sources. The observations thus extend over nine orbits of EXO 0748−676, and total 38,500 s, excluding periods of Earth occultation. The first day of the observation was performed in MPC2 mode, with a maximum time resolution of 0.0625 s; for the remainder MPC1 was utilized, with time resolutions of 0.5 and 16 s. A standard background subtraction was performed on the data. Figure 2 contains the light curve.

## 3. TEMPORAL ANALYSES

### 3.1. *The XB 1916−053 Light Curve*

#### 3.1.1. *Period Determination*

We have applied the standard periodicity analyses to this new *Ginga* data set, in order to obtain a further independent determination of the X-ray period, Using a periodogram search technique, we derive a period of 3000 ± 5 s, consistent with previous X-ray measurements (see Paper II for a summary of all period determinations of XB 1916−053) but inconsistent with the well-defined optical period of 3027.5 ± 0.2 s (Grindlay et al. 1988; Grindlay 1989). We display the light curve folded on the 3000 s period in the upper panel of Figure 3*a*. In the lower panel, we show the number of samples that contributed to each phase bin; the uneven sampling distribution is due to the beating of the 50 minute period of the system with the orbital period of the *Ginga* satellite.

© American Astronomical Society • Provided by the NASA Astrophysics Data System

1992ApJ...400..330S



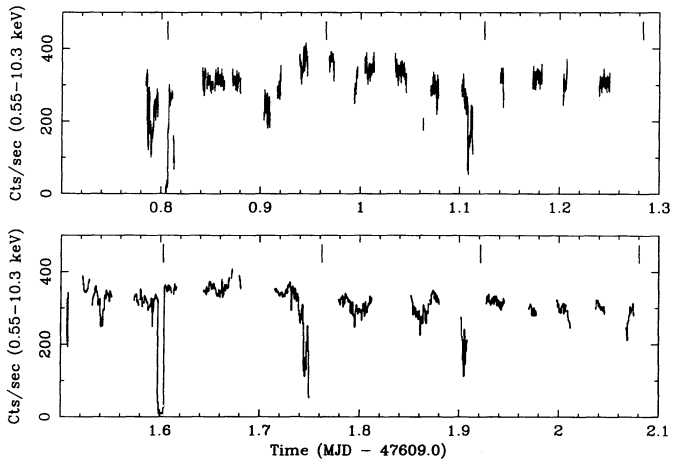


FIG. 2.—The light curve from the *Ginga* observation of EXO 0748−676 in 1989 March, summed into 64 s time bins. The expected times of eclipse by the secondary star are indicated on the figure.

### 3.1.2. *Dip Evolution*

Primary dipping activity is observed through most of the observation. In addition to this, strong secondary dips are visible during the first day, at a phase of 0.55 relative to the primary dips. A careful visual inspection of the light curve (Fig. 1), and the results of folding analysis on various subsets of the data, indicate that changes in the shapes and positions of the dips were occurring during the observation. Because of the numerous data gaps, it is not easy to show this effect in a conventional manner. Therefore, we have produced light curves by phase bin; for each bin we search the observation for data segments that fall within that bin. These segments are plotted against time; when the particular phase interval is not observed for many orbital cycles, this will show up as a gap in the long-term light curve of that bin. In this way the phase-related variations become evident.

Figure 4 is a set of such plots for a period of 3000 s, in 20 phase bins. In this representation, phase bins 4–7 and 14–16 are the quiescent (no dip) intervals, indicated by the fact that whenever there are data, they are at the same level. The center of primary dipping activity occurs in bins 20, 1, and 2; dipping activity in these phase intervals starts 20,000 s after the beginning of the *Ginga* observation and persists until the end. In bins 9–11 we see the secondary dips evident in the light curve. However, these dips do not hold their position in phase; the time at which secondary dipping activity peaks in panel 9 is ~30,000 s earlier than in panel 10, demonstrating that the dip center shifts by 0.05 of a cycle over ~10 orbits of the system. Dipping also persists longer in bin 11 than in 10 by 10,000 s.

We have examined a similar set of plots for a period of 3027 s and find that neither the primary nor the secondary dips stay at a constant phase, a further indication that the optical and X-ray periods are indeed different, and that the optical period of 3027 s is inappropriate for use with the X-ray data.

### 3.2. *The EXO 0748−676 Light Curve*

In our observation of EXO 0748−676 the source was found to be in a bright state with a 1–20 keV flux of $8.8 \times 10^{-10}$ ergs $cm^{-2}$ $s^{-1}$, comparable to its maximum observed brightness in previous observations. Examining the light curve, two eclipses are evident at MJDs of 47609.806 and 47610.603, corresponding to $N = 9406$ and $N = 9411$ using the ephemeris of Parmar et al. (1986). The second eclipse was observed with the highest time resolution (0.0625 s), and has a well-defined ingress and egress. The duration of this eclipse is 490.2 ± 1.0 s, with ingress and egress durations of 9.4 ± 1.0 s and 8.7 ± 1.0 s, respectively. (The large errors on these durations relative to the time resolution of the data are due to the intrinsic variability of the source before and after eclipse.) During this second eclipse, flux is still present at a level of 2.8% ± 0.1% of the nearby quiescent flux in the 1–10 keV band and 4.5% ± 2.5% for the 10–20 keV band. During the deepest part of the eclipse the count rate is consistent with a constant source, with a $\chi^2_\nu$ of 0.57.

The *Ginga* coverage of the light curve of EXO 0748−676 is sufficient to enable an independent determination of its orbital period to be made. Using a standard period-folding program we find a maximum in the $\chi^2$ distribution corresponding to an

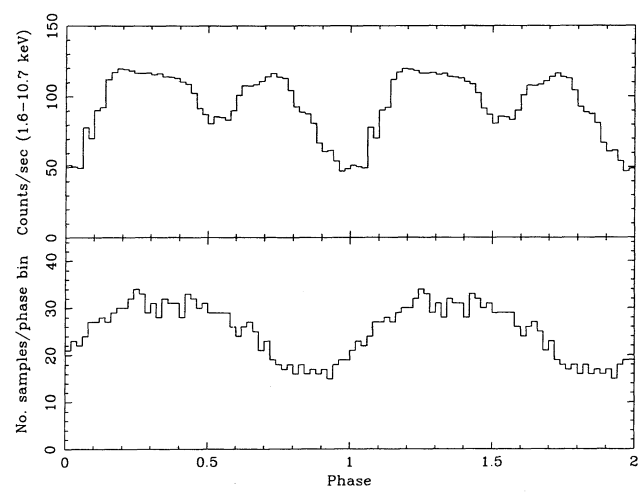


FIG. 3a

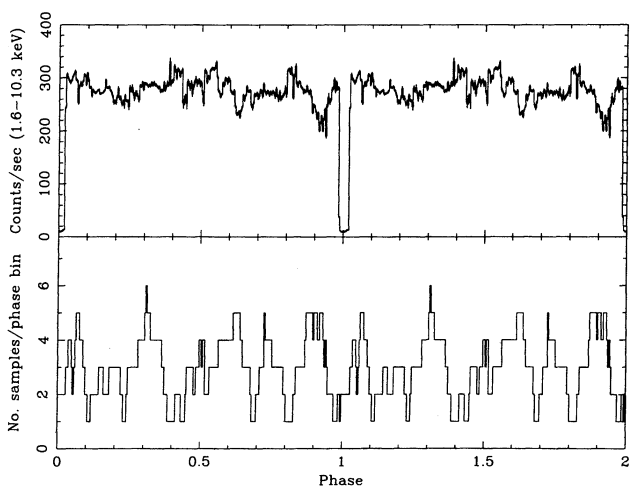


FIG. 3b

FIG. 3.—Folded light curves from the two observations. In each case the upper panel contains the light curve folded on the orbital period, while the lower panel shows the number of times each phase bin was sampled. (*a*) For XB 1916−053 the data were folded into 50 phase bins. The primary and secondary dips are clearly shown. The beating of the 50 minute orbital period with the orbital period of the *Ginga* satellite is evident in the lower panel. (*b*) The data from EXO 0748−676 were folded into 250 phase bins. In addition to the eclipse at phase zero, note the dips at phases 0.9, 0.63, and 0.2.

© American Astronomical Society • Provided by the NASA Astrophysics Data System

1992ApJ...400..330S



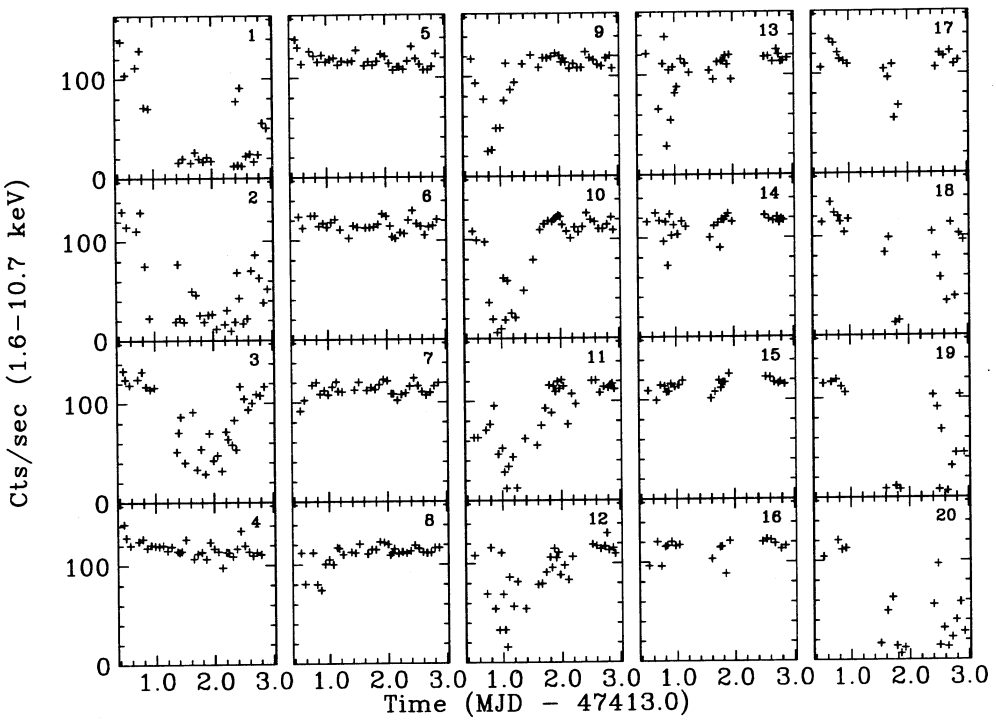


FIG. 4.—The XB 1916−053 light curves plotted by phase bin for a period of 3000 s (see text). The error bars are smaller than the symbols used, and the contributions from the bursts have been removed.

orbital period of 3.835 ± 0.026 hr. Using the eclipses as fiducial markers we can improve this estimate to 3.82391 ± 0.00022 hr, consistent with (but less precise than) the original *EXOSAT* value (Parmar et al. 1986). In all, nine observations of EXO 0748−676 were performed using *EXOSAT*, including 30 well-determined eclipses. Combining the eclipse times from *EXOSAT* with the *Ginga* data described here, Parmar et al. (1991) have refined the ephemeris of EXO 0748−676 and shown that the orbital period of EXO 0748−676 is decreasing on a time scale of $5 \times 10^6$ yr.

In addition to the eclipses, the light curve contains several prominent dips at phases 0.90, 0.63, and 0.20. Our coverage includes four dips at phase $\phi = 0.9$, with maximum flux reductions in the range 50%–80%; three dips at $\phi \sim 0.6$ with maximum depths of ~30%–40%; and one at $\phi = 0.2$ with a depth of 33%. Additional low-level variability is clear in the folded light curve, shown in Figure 3*b*.

## 4. SPECTRAL ANALYSIS

### 4.1. *Quiescent Spectra*

The nondipping, nonbursting ("quiescent") spectrum of XB 1916−053 was accumulated for three separate data intervals during the 1988 September observation. Since dip activity potentially occurs for a wide range of orbital phase, the quiescent data were selected using a hardness ratio (6–10 keV/2–6 keV) as a discriminator. For comparison, we also extracted a quiescent spectrum from the 1987 September observation (see Paper II for more details of these data). Similar results were obtained from both data sets.

The quiescent spectrum resembles a power law, and although a single power-law fit is unacceptable ($\chi^2_\nu \sim 11$), the measured photon index of −1.9 is similar to those measured from the *EXOSAT* data. A variety of other models (thermal bremsstrahlung, generalized thermal, power-law plus blackbody, thermal plus blackbody, etc.) also gave poor fits to the data, as demonstrated in Table 1A. As no physically convincing parameterization could be achieved, we adopted a model consisting of a power law and a broad Gaussian line in our analysis of the dip spectra. We caution that this model should not be overinterpreted and is used solely to parameterize the data. In the analysis of the bursts, the deviation from a power law is insignificant relative to the magnitude of the blackbody component (see below).

A simple power law was found to be a good fit to quiescent spectra obtained with *EXOSAT* and some earlier satellites. This is not the case with the current data, where a power-law fit results in a large residual at low energies. We have investigated and excluded several possibilities for this feature. First, it is not due to mixing of dip and nondip data, as strenuous efforts were made to separate these intervals. Second, it cannot be explained as a consequence of inaccurate pointing by *Ginga*. During this observation the source was off-axis by an average of 24′, which is not an unusually large value (and is in fact slightly smaller than the 30′ off-axis angle for the EXO 0748−676 observation). Such an offset will affect the spectrum by a few percent, but the effect we see is a factor of 5 larger than this. In addition, the spectrum does not have the characteristic shape associated with a collimator reflection component. Third, our background-subtraction method cannot be responsible; any problems here would show up as differences between the LAC top- and middle-layer data, which we do not see. The only remaining possibilities are (1) that a contaminating source was within the LAC field of view and (2) that the change in the source spectrum is genuine.

The first possibility cannot be discounted, although no nearby contaminating source is seen in *EXOSAT* or *Einstein* images or suggested by any other previous observation. In

© American Astronomical Society • Provided by the NASA Astrophysics Data System

1992ApJ...400..330S



TABLE 1A

THE QUIESCENT SPECTRUM OF XB 1916−053

A.

| Model | $A_1 \times 10^{-2}$ | $\alpha$ | $E_0$ (keV) | $E_c$ (keV) | $N_H$ ($\times 10^{21}$ cm$^{-2}$) | $\chi^2$/dof |
|---|---|---|---|---|---|---|
| Power-law | $6.59^{+0.39}_{-0.37}$ | $1.89^{+0.03}_{-0.03}$ | ... | ... | $10.3^{+1.5}_{-1.5}$ | 260/23 |
| Power-law + cutoff | $3.73^{+0.64}_{-0.45}$ | $1.53^{+0.12}_{-0.10}$ | $5.4^{+0.4}_{-0.5}$ | $19^{+7}_{-3}$ | $0.75^{+3.13}_{-0.75}$ | 114/21 |

B.

| Model | $A_1 \times 10^{-2}$ | $kT_1$ (keV) | $A_2 \times 10^{-2}$ | $kT_2$ (keV) | $N_H$ ($\times 10^{21}$ cm$^{-2}$) | $\chi^2$/dof |
|---|---|---|---|---|---|---|
| Thermal bremsstrahlung | $1.70^{+0.08}_{-0.06}$ | $15.05^{+0.71}_{-0.76}$ | ... | ... | $0.59^{+1.16}_{-0.59}$ | 165/23 |
| Thermal bremsstrahlung + blackbody | $1.36^{+0.19}_{-0.12}$ | $17.5^{+2.7}_{-4.0}$ | $0.82^{+0.82}_{-0.52}$ | $1.20^{+0.22}_{-0.15}$ | $0.0^{+0.8}_{-0.0}$ | 142/21 |

C.

| Model | $A_1 \times 10^{-2}$ | $\alpha$ | $A_2 \times 10^{-2}$ | $kT_2$ (keV) | $N_H$ ($\times 10^{21}$ cm$^{-2}$) | $\chi^2$/dof |
|---|---|---|---|---|---|---|
| Power-law + blackbody | $3.51^{+0.59}_{-0.28}$ | $1.70^{+0.06}_{-0.04}$ | $0.088^{+0.032}_{-0.030}$ | $1.51^{+0.13}_{-0.11}$ | $0.0^{+1.9}_{-0.0}$ | 96/21 |

D.

| Model | $A_1 \times 10^{-2}$ | $\alpha$ | $E_l$ (keV) | $\Delta E_l$ (keV) | $N_H$ ($\times 10^{21}$ cm$^{-2}$) | $\chi^2$/dof |
|---|---|---|---|---|---|---|
| Power-law + line | $5.10^{+0.85}_{-0.73}$ | $1.81^{+0.06}_{-0.06}$ | $5.60^{+0.53}_{-0.43}$ | $1.39^{+0.64}_{-0.44}$ | $4.6^{+2.7}_{-3.4}$ | 37/20 |

NOTE.—The functional form of the power-law + cutoff model is $S = AE^{-\alpha} \exp -(E - E_0)/E_c$.

support of the second possibility, we note that White & Swank (1982) presented *OSO 8*, *HEAO 1* A-2, and *Einstein* observations of XB 1916−053 and noted that the spectrum shape was softer during the *HEAO 1* observation, the best fit being a bremsstrahlung model with $kT \sim 12$ keV. It therefore seems possible that we have again caught the system in an unusual state.

We have fitted the quiescent spectrum of EXO 0748−676 with rather more success. A variety of models were tried, including power-law, bremsstrahlung, power-law plus high-energy cutoff (generalized thermal), and power-law plus blackbody (see Table 1B). We find that over the energy range 1.5–36 keV the best fit is achieved by the generalized thermal model ($S = AE^{-\Gamma}e^{-E/kT}$), with parameters of $\Gamma = 1.9 \pm 0.1$, $kT = 8.3^{+1.4}_{-1.1}$ keV, and $N_H = (5.9^{+1.9}_{-1.4}) \times 10^{21}$ cm$^{-2}$, (90% confidence errors are quoted on all parameters and a systematic error of 0.5% was included in all fits.) These values are consistent with the parameters derived by Parmar et al. (1986).

### 4.2. *Dip Spectra*

Dip spectra were selected from the observations of XB 1916−053 and EXO 0748−676 on the basis of source intensity in the 2–11 keV band. A spectral integration time of 4 s was used for the XB 1916−053 data, and 16 s for EXO 0748−676.

Since the dip variability occurs on time scales as short as a few seconds, it may be expected that the results will be sensitive to the intrinsic time binning of the data. However, for high time resolution data, the errors in determination of the flux used to select the spectra become large, which would also lead to mixing of different spectral states within a chosen intensity

TABLE 1B

THE QUIESCENT SPECTRUM OF EXO 0748−676

A.

| Model | $A_1$ | $\alpha$ | $E_0$ (keV) | $E_c$ (keV) | $N_H$ ($\times 10^{21}$ cm$^{-2}$) | $\chi^2$/dof |
|---|---|---|---|---|---|---|
| Power-law | $1.0^{+\infty}_{-0.95}$ | $2.8^{+0.3}_{-2.8}$ | ... | ... | $19.7^{+0.9}_{-19.7}$ | 617/42 |
| Power-law + cutoff | $0.89^{+0.05}_{-0.04}$ | $2.77^{+0.03}_{-0.02}$ | $15.7^{+0.7}_{-0.6}$ | $1.0^{+0.6}_{-0.2}$ | $16.6^{+1.2}_{-0.9}$ | 511/40 |

B.

| Model | $A_1$ | $kT_1$ (keV) | $E_0$ (keV) | $E_c$ (keV) | $N_H$ ($\times 10^{21}$ cm$^{-2}$) | $\chi$/dof |
|---|---|---|---|---|---|---|
| Thermal bremsstrahlung | $0.167^{+0.002}_{-0.002}$ | $4.96^{+0.05}_{-0.05}$ | ... | ... | $0.0^{+0.28}_{-0.0}$ | 377/42 |

C.

| Model | $A_1$ | $\alpha$ | $A_2 \times 10^{-3}$ | $kT_2$ (keV) | $N_H$ ($\times 10^{21}$ cm$^{-2}$) | $\chi$/dof |
|---|---|---|---|---|---|---|
| Power-law + bremsstrahlung | $1.00^{+0.17}_{-0.13}$ | $2.98^{+0.11}_{-0.09}$ | $1.59^{+0.45}_{-0.33}$ | $1.69^{+0.11}_{-0.12}$ | $15.8^{+2.2}_{-2.2}$ | 87/40 |

D.

| Model | $A_1$ | $\Gamma$ | $A_2 \times 10^{-3}$ | $kT$ (keV) | $N_H$ ($\times 10^{21}$ cm$^{-2}$) | $\chi$/dof |
|---|---|---|---|---|---|---|
| Generalized thermal | $0.42^{+0.06}_{-0.04}$ | $1.9^{+0.1}_{-0.1}$ | ... | $8.3^{+1.4}_{-1.1}$ | $5.9^{+1.9}_{-1.4}$ | 80/41 |

© American Astronomical Society • Provided by the NASA Astrophysics Data System

1992ApJ...400..330S



band. The data from the two sources considered here have been selected at the maximum consistently available time resolution, and the intensity bands chosen such that the errors in the flux determination were small compared to the selection window. Typically the intensity states were divided into about 10–15 bands of equal width.

Modeling these spectra with a simple absorption of the high-state spectrum proved unsuccessful, giving $\chi^2_\nu > 2$ for the dip spectra. Inspection of the fits to this model showed that the cause was an excess of counts at low energies, as also found in earlier work (Paper I; Parmar et al. 1986).

The dip spectra were then fitted using a variation on a two-component model previously found to be successful on this and other dipping sources (see, e.g., Parmar et al. 1986 and Paper I). Each component has the same continuum shape as the quiescent spectrum, with one $N_H$ fixed at the quiescent value and the other allowed to vary as a free parameter. The two normalizations are the only other free parameters. This model was found to provide a good fit to all the dip spectra, with $\chi^2_\nu$ in all cases less than 1.5.

An example of a two-component fit to a spectrum from XB 1916−053 in an intermediate intensity level is shown in Figure 5, and in Figure 6 we show the behavior of the derived parameters from a series of two-component fits to intensity-selected spectra from our two sources illustrating the trends seen in all analyzed sections. For XB 1916−053 above 80 counts $s^{-1}$ and EXO 0748−676 above 200 counts $s^{-1}$, the spectrum can be represented by a single component, and if a two-component fit is used the normalizations of the components cannot be constrained in the fitting routine. Below these thresholds, the parameters vary with dip depth in a similar way for each source; the column density of the absorbed ("variable $N_H$") component increases with decreasing flux from its quiescent value of a few $\times 10^{21}$ $cm^{-2}$ to maximum values of $\sim 7 \times 10^{23}$ $cm^{-2}$ and $2.2 \times 10^{23}$ $cm^{-2}$, respectively, for XB 1916−053 and EXO 0748−676. The normalization of the fixed absorption component appears to decrease approximately exponentially with dip depth, and the normalization of the variable absorption component shows more complex behavior, with a maximum value occurring at intermediate intensities.

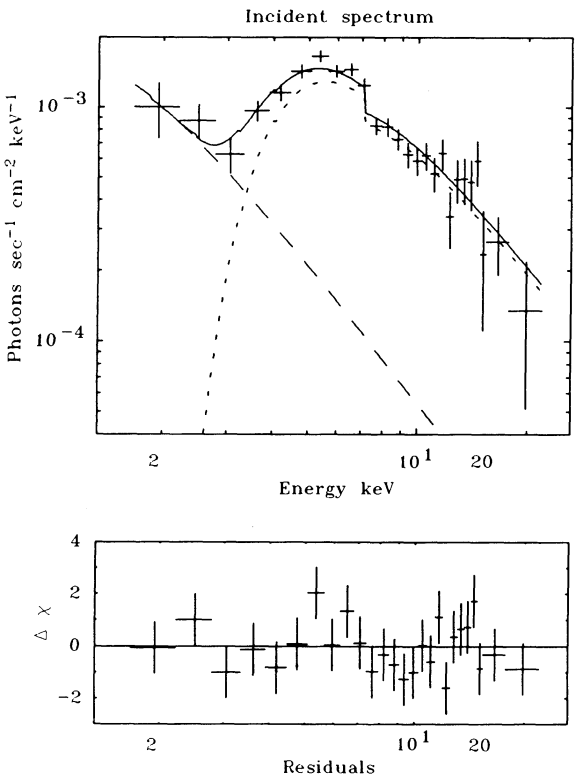


FIG. 5.—An example of a two-component fit to the *Ginga* data from XB 1916−053. This spectrum was accumulated in the intensity band covering 25–35 counts $s^{-1}$. One component has the same continuum shape as the quiescent continuum but is heavily absorbed by the material in the disk bulge. The second component represents the contribution to the spectrum from scattering.

There are several physical situations which may result in this type of spectral behavior. A low-energy component may arise if the absorbing medium is partially ionized. A similar effect is also possible if the absorbing medium has a peculiar composition. If the source is physically extended and partially covered, the emergent spectrum will have two components, and the normalizations of the fixed and variable absorption components ($A_{fix}$ and $A_{var}$) will be related to the normalization of the unabsorbed source spectrum ($A_0$) in the following way:

$$A_0 = A_{fix} + A_{var} \exp(rN_{Hvar}\sigma_T) .$$

The quantity $r$ is the ratio of electron to measured hydrogen column densities $N_e/N_{Hvar}$, which is a measure of the metallicity of the absorbing medium. In a partial covering model, if $A_0$, $A_{fix}$, and $A_{var}$ can be measured, the metal abundance of the medium can be determined. In this way, we derive metal abundances $1/r$ of $0.5 \pm 0.1$ for XB 1916−053 and $0.5 \pm 0.3$ for EXO 0748−676 (90% confidence), consistent with previous determinations (XB 1916−053: 0.2–1.0, Paper I. EXO 0748−676: 0.1–0.5, Parmar et al. 1986).

### 4.3. *Dip Spectra—Simulations*

An instrumental interpretation of the two-component fit was suggested by Parmar et al. (1986), who recognized that if the source exhibits simple absorption, and this column density changes on time scales shorter than the instrumental spectral accumulation time, the resultant spectrum could contain an excess of soft flux over the best-fitting simple absorption model, which in the two-component parameterization may show up as an addition to the normalization of the unabsorbed component. Inspection of our data from both XB 1916−053 and EXO 0748−676 shows that dip transitions and flux variations occur on faster time scales than the minimum possible spectral integration times used, and that this may be a viable alternative interpretation for our data. To investigate this suggestion in more detail, we have performed a series of simulations of dip spectra.

The object of the exercise was to generate the pulse height spectra that would be observed with the LAC given a spectrum with time-variable normalization and column density. These data were then analyzed in the same manner as the real data. The intrinsic spectrum chosen for the simulation was a power law with photon index 1.9, approximating closely to the spectrum of XB 1916−053. A reference set of 500 pulse height spectra was generated by folding this spectrum through the detector response for a wide range of column densities, with $N_H = (1–500) \times 10^{21}$ $cm^{-2}$. Given a model of the time behavior of the column and normalization, the spectrum at any time could be found by choosing the nearest $N_H$ value in the reference set and scaling it to account for the attenuation due to

© American Astronomical Society • Provided by the NASA Astrophysics Data System

1992ApJ...400..330S



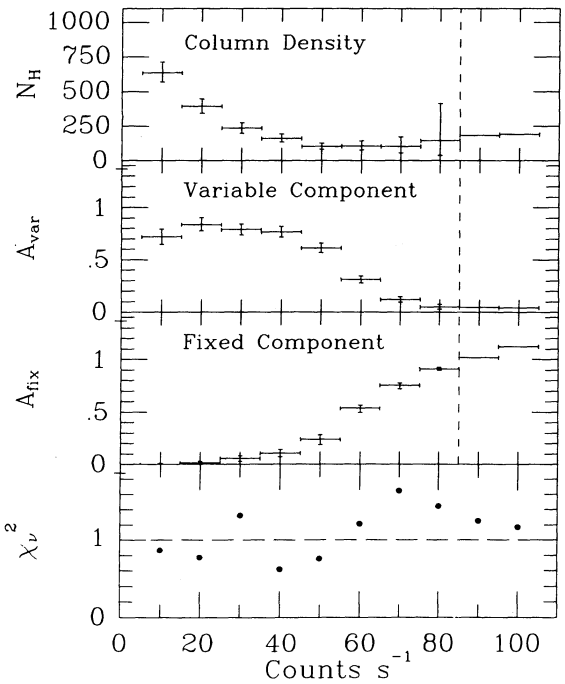


FIG. 6a

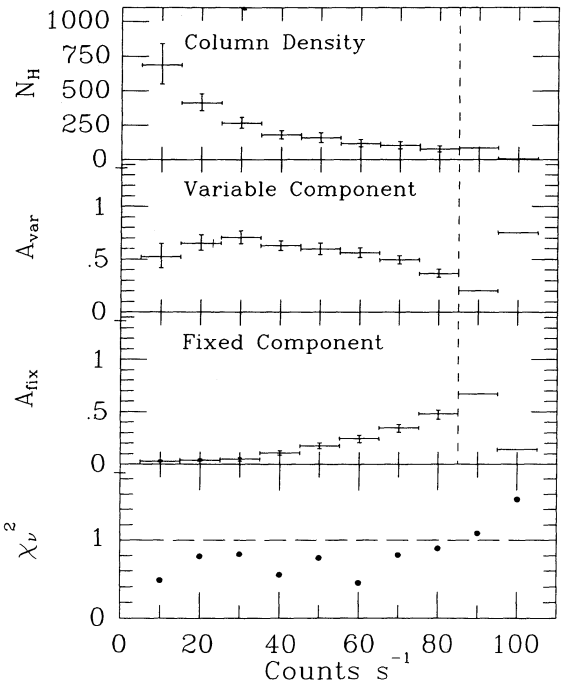


FIG. 6b

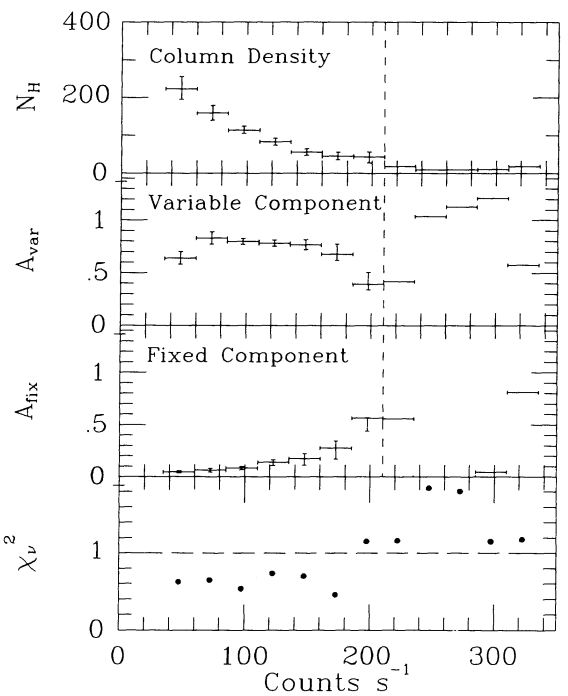


FIG. 6c

FIG. 6.—The parameters derived from two-component fits to intensity-selected spectra from the two sources. (*a*) The data from the 1987 September observation of XB 1916−053. (*b*) The data from the 1988 September observation of XB 1916−053. (*c*) The data from the 1989 March observation of EXO 0748−676. In all three cases, note the similarities: a strong increase in the $N_H$ of the absorbed component and a decrease in the normalization of the scattered (or "fixed $N_H$") component with decreasing countrate. Above 80 counts s$^{-1}$ for XB 1916−053 and 200 counts s$^{-1}$ for EXO 0748−676 the two components become indistinguishable and error bars cannot be assigned.

energy-independent electron scattering that would be expected given the metal abundance of the model absorbing medium.

To simulate dip variability, we assumed a linear dependence of $N_H$ with time during the ingress and egress to dips, using the simple periodic waveform shown in Figure 7, with $N_H$ in the range (2–500) × $10^{21}$ cm$^{-2}$ and a period denoted by $P_{N_H}$. The artificial spectra were calculated at a time resolution of 0.125 s and accumulated into bins of 4 s duration, i.e., 32 "intrinsic" spectra per "observed" output spectrum. We studied two different variability time scales for the column density. In the first, a period of $P_{N_H} = 1000$ s was chosen, representing the case where the $N_H$ variability is slow compared to the spectral sampling time. We predicted that in this case, the mixing effect should be small. In the second, we used $P_{N_H} = 50$ s, thus simulating fast $N_H$ variations, as a full dip transition occurs in about three time bins.

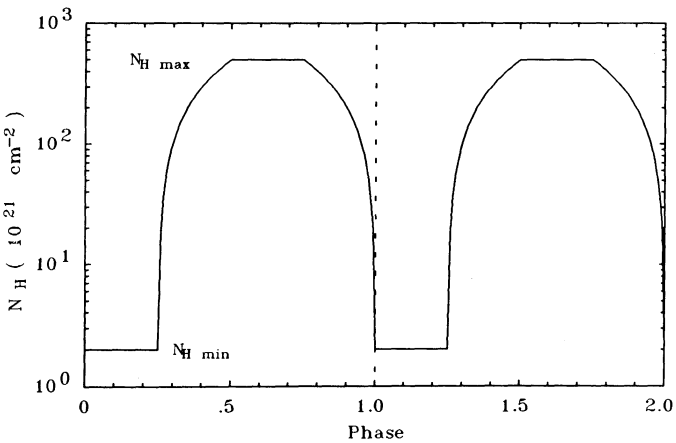


FIG. 7.—The variations of $N_H$ used in the simulations of the dip spectra (see text).

© American Astronomical Society • Provided by the NASA Astrophysics Data System

1992ApJ...400..330S



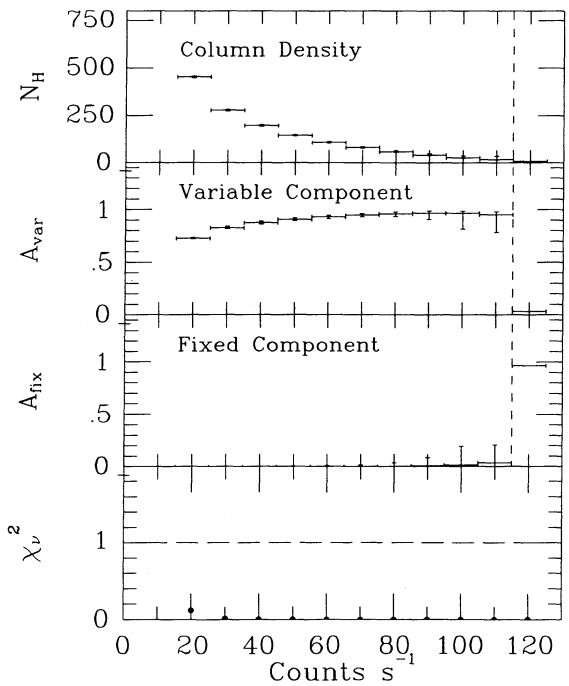


FIG. 8a

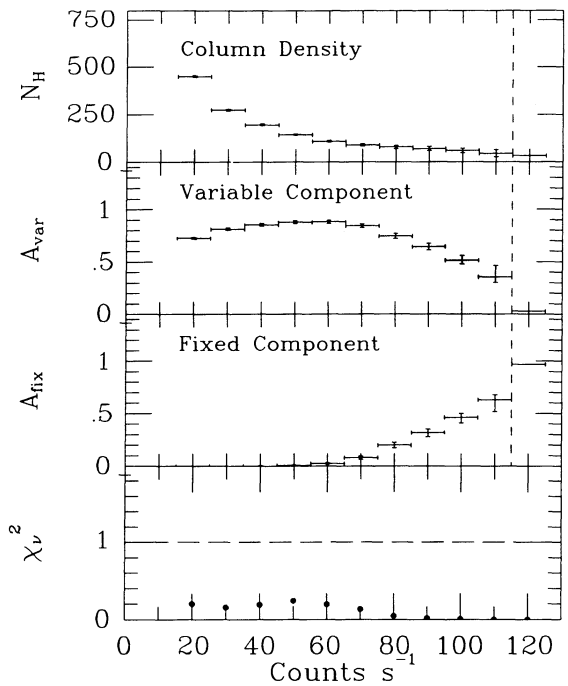


FIG. 8b

FIG. 8.—The parameters derived from a two-component fit to simulated XB 1916−053 data. (*a*) The case where the dip transition time is slow compared to the spectral integration time; spectra reduce to a simple absorbed component. (*b*) The case where the dip transition time is fast; compare these to the diagrams derived from real data in Fig. 6.

The case of slow $N_H$ variability is shown in Figure 8*a*. The behavior of the model parameters is much as anticipated. For all dipping count rates, the normalization of the fixed-absorption component is effectively zero, indicating that a one-component model is a good fit to the data. The column density decreases exponentially with increasing flux, as might be expected, and the normalization of the variable absorption component also behaves exponentially, as the flux is removed by energy-independent electron scattering as the column increases.

For fast $N_H$ changes, however, it can be seen from Figure 8*b* that the behavior of the model parameters is similar to that observed in real dip sources. The column density increases approximately exponentially with dip depth, the fixed-absorption component shows decreasing normalization with decreasing flux, and the variable component normalization shows a maximum at intermediate flux values.

We conclude that the simulations show that the two-component model gives a good representation of a spectrum that undergoes rapid changes in column density. Although the simulations shown here were based on an approximation to the spectrum of XB 1916−053, the conclusions are equally valid for EXO 0748−676 and indeed for any reasonable "intrinsic" source spectrum.

The above simulations were repeated using different assumed metal abundances in the absorbing medium. For fast $N_H$ changes, it was found that the parameters of the two-component model behave as if the source were in fact partially covered. Thus, the metal abundance of the absorbing material in dip sources may still be calculated using the equation in the previous section, and our conclusions about the abundances in the two sources are unchanged.

Discrimination between genuine partial covering and the mixing effect is, however, extremely difficult. Inspection of the residual patterns to the spectral fits to mixed spectra indicates that *Ginga* observations of any dip source could not distinguish between partial covering and spectral mixing, provided that the mixing occurs at $\lesssim$ the minimum time resolution. In the simulations of XB 1916−053, it was found that the maximum expected difference between the two models would be $\approx 0.05$ counts $s^{-1}$ per PHA channel. Even scaling up to the brightest dip sources would show residuals of only $\approx 0.25$ counts $s^{-1}$ $PHA^{-1}$, similar to the systematic residuals in the *Ginga* quiescent spectra of LMXBs.

To summarize: where the linear dip transition time is slow compared to the integration time ($\sim 50$ integration bins), the two-component model reduces to the case of simple absorption, as expected. However, in the case where the dip transition time scale is similar to the integration time scale, a two-component fit is required, with similar general trends to those seen in real dip data. This is illustrated in Figure 8 for the "slow" and "fast" cases, respectively.

### 4.4. *Burst Spectra*

No bursts were observed from EXO 0748−676 during the *Ginga* observations. Gottwald et al. (1986) observed 26 bursts in a total of $3.7 \times 10^5$ s of *EXOSAT* observations, implying a mean burst frequency of 0.25 burst $hr^{-1}$. This frequency is, however, found to be strongly anticorrelated with the level of the persistent emission, ranging from 0.12 burst $hr^{-1}$ when the source is brighter than $7.5 \times 10^{-10}$ ergs $cm^{-2}$ $s^{-1}$ to 0.56 burst $hr^{-1}$ when $F_x < 5.0 \times 10^{-10}$ ergs $cm^{-2}$ $s^{-1}$. (The maximum burst recurrence time observed in the *EXOSAT* data is >57,000 s.) In the flux regime we observe, we might expect about four bursts to occur during the time span of the observation. Considering that during our observations we actually

© American Astronomical Society • Provided by the NASA Astrophysics Data System

1992ApJ...400..330S



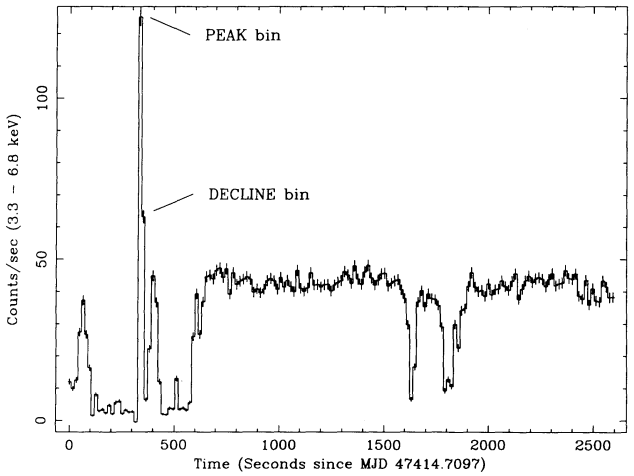


FIG. 9.—Here we show the second burst observed from XB 1916−053, which occurs during a dip, with 16 s time resolution. The time bins used to obtain the PEAK and DECLINE spectra referred to in the text are marked.

have data for 31% of the time, the lack of bursts in our data is not inconsistent with these numbers.

Three bursts were detected during the observation of XB 1916−053, at phases 0.57, 0.07, and 0.15. The first burst has been excluded from analysis, since its rise was not observed. The second burst occurs during a dip (see Fig. 9). We have performed a careful investigation of this burst and compared its properties to those derived from the third burst, which occurred during a quiescent interval. Both of the analyzed bursts occurred during intervals when the time resolution of the data was 16 s.

#### 4.4.1. *XB 1916−053 Burst 3 ("Normal", Out-of-Dip)*

Spectra were accumulated for the 16 s bin containing the burst peak ("PEAK") and the next 16 s bin ("DECLINE"). For these sources, where there is no evidence for the presence of the neutron star photosphere in the quiescent spectrum, conventional wisdom states that the spectra accumulated during bursts are the sum of the quiescent spectrum from the disk plus a blackbody-line contribution from the thermonuclear flash on the neutron star. Thus, the average quiescent spectrum is usually subtracted from the burst spectra and the result fitted with a blackbody. We followed this standard approach for our first pass through the data.

The results of blackbody fits to the quiescent-subtracted spectra, PEAK − Q and DECLINE − Q, are shown in Table 2A. $N_H$ is fixed at the *EXOSAT* quiescent value; although a lower column density does improve the fit marginally, it is not well constrained by the data, and fits with $N_H$ left as a free parameter fail to converge. In both the PEAK − Q and DECLINE − Q spectra, significant excess flux is seen both at the lowest and highest energy bands with respect to the best-fit blackbody, leading to the poor $\chi^2_\nu$ values (>2) we obtain. Other single-component fits are even less successful in describing the data, with $\chi^2_\nu \sim 10$.

In an effort to improve the spectral fits, we tried a combination of blackbody and power-law components, and obtained much more acceptable values for $\chi^2_\nu(<1$; see Table 2A). From these results we deduced that our original assumption of a constant disk emission component was erroneous, and that the additional power-law component may be interpreted as a brightening of the component from the disk.

In Figure 10 we show the results of fitting a power-law plus blackbody model to the PEAK and DECLINE spectra *without* first subtracting the quiescent component. For both spectra the fits are acceptable, with $\chi^2_\nu \sim 1$. The derived blackbody temperatures are indistinguishable from those determined from the previous quiescent-subtracted spectral fits, and the power-law photon index is identical to that of the quiescent emission, within the errors. However, the total flux in the power-law component is greater than the quiescent flux by a factor of 2.7 for the PEAK spectrum and 1.8 for the DECLINE.

#### 4.4.2. *XB 1916−053 Burst 2 (in a Dip)*

As far as we are aware, this is the first time that spectral analysis of a burst in a dip has been attempted. We therefore tried several different approaches to the problem. Our initial approach was to accumulate PEAK and DECLINE spectra for the relevant time bins, as for burst 3, and then create two different background-subtracted spectra for each time interval. "PEAK − D" refers to the spectrum in which the average of

TABLE 2A

THE SPECTRUM OF BURST 3 (OUT OF DIP)

| Spectrum | Model | $\chi^2_\nu$ (dof) | $A \times 10^{-2}$ | $kT$ (keV) or $\alpha$ | $N_H(\times 10^{21}$ cm$^{-2})$ |
|---|---|---|---|---|---|
| PEAK − Q ..... | BB | 2.77 (43) | $1.01^{+0.07}_{-0.07}$ | $2.19^{+0.05}_{-0.05}$ | 2.1 (fixed; <1.0) |
| | PL | 8.68 (42) | 84.0 | 1.96 | 65.0 (free) |
| | TB | 10.13 (43) | 43.8 | 50.0 | 31.0 (free) |
| | BB + PL (BB) | 0.90 (41) | $0.72^{+0.16}_{-0.11}$ | $2.27^{+0.12}_{-0.14}$ | |
| | (PL) | | $6.70^{+7.30}_{-3.26}$ | $1.61^{+0.89}_{-1.03}$ | 2.1 (fixed; <33.0) |
| DECLINE − Q ..... | BB | 2.20 (43) | $3.77^{+0.63}_{-0.32}$ | $1.16^{+0.05}_{-0.04}$ | 2.1 (fixed; < 3.0) |
| | BB + PL (BB) | 0.87 (41) | $3.94^{+1.60}_{-1.57}$ | $1.07^{+0.09}_{-0.10}$ | |
| | (PL) | | $3.38^{+6.76}_{-3.03}$ | $1.57^{+0.52}_{-0.87}$ | 2.1 (fixed; <81.0) |
| PEAK[a] ..... | BB + PL (BB) | 0.95 (41) | $0.74^{+0.06}_{-0.07}$ | $2.26^{+0.09}_{-0.09}$ | |
| | (PL) | | $16.7^{+4.6}_{-3.0}$ | $1.83^{+0.30}_{-0.19}$ | 2.1 (fixed; <8.0) |
| DECLINE[a] ..... | BB + PL (BB) | 1.05 (41) | $2.83^{+1.31}_{-0.83}$ | $1.04^{+0.09}_{-0.08}$ | |
| | (PL) | | $13.0^{+3.3}_{-3.1}$ | $1.93^{+0.11}_{-0.04}$ | 2.1 (fixed[b]) |

[a] No quiescent subtraction.

[b] Best fit requires a column of $25.0^{+8.6}_{-7.4} \times 10^{21}$ cm$^{-2}$ with a power-law slope much steeper (~2.7) than in quiescence.

© American Astronomical Society • Provided by the NASA Astrophysics Data System

1992ApJ...400..330S



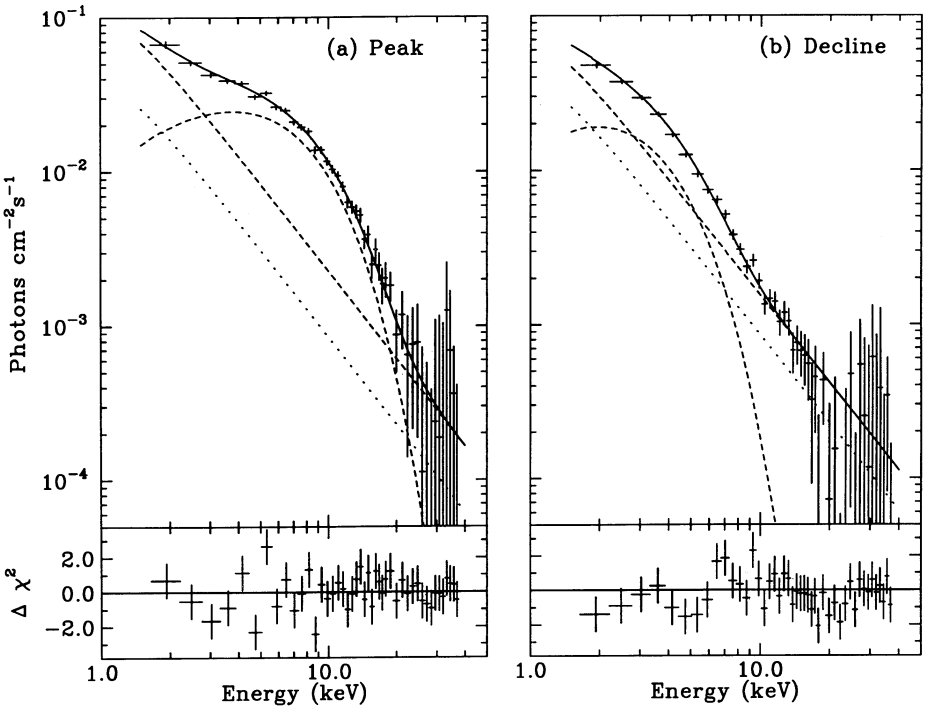


FIG. 10.—Spectral fits to the PEAK and DECLINE spectra for burst 3, a "normal" burst observed outside a dip interval. No quiescent spectrum has been subtracted from these spectra prior to fitting. In each panel, the solid line shows the best-fitting power-law plus blackbody model. The dashed lines show the contribution that each of these components makes to the total spectrum, and the dotted line indicates the spectrum of the quiescent emission before the burst.

the lowest count rate dip spectrum has been subtracted from the raw "PEAK" spectrum; for "PEAK − Q", the average quiescent (nonbursting, nondipping) spectrum has been subtracted.

Fitting these spectra with single-component models, we again found that power-law or thermal bremsstrahlung fits were very poor, with $\chi^2_\nu > 10$, and that a single blackbody fit was also formally unacceptable. For the PEAK − D spectrum, $N_H$ does not converge, and we therefore fixed it at two trial values and present both results in Table 2B. Our principal result from these fits is that regardless of whether the quiescent or the dip spectrum is subtracted, *the data are inconsistent with a high* ($\sim 10^{23}$ cm$^{-2}$) *column density*. The best-fit model gives a quiescent (out-of-dip) column, and the fit to PEAK − Q is

TABLE 2B

THE SPECTRUM OF BURST 2 (IN A DIP)

| Spectrum | Model | $\chi^2_\nu$ (dof) | $A \times 10^{-2}$ | $kT$ (keV) or $\alpha$ | $N_H$( $\times 10^{21}$ cm$^{-2}$) |
|---|---|---|---|---|---|
| PEAK − D | BB | 5.59 (43) | 0.88 | 2.52 | 10.0 (fixed) |
| | | 3.77 (43) | 0.80 | 2.58 | 2.1 (fixed) |
| | BB + PL (BB) | 1.71 (40) | $0.61^{+0.11}_{-0.07}$ | $2.65^{+0.15}_{-0.16}$ | |
| | (PL) | | $3.63^{+4.37}_{-2.19}$ | $1.22^{+0.99}_{-1.53}$ | 0.14 (free; <20.0) |
| DECLINE − D | BB | 2.12 (42) | $1.14^{+0.12}_{-0.11}$ | $1.71^{+0.08}_{-0.08}$ | 7.4 (free; <15.7) |
| | BB + PL (BB) | 1.64 (40) | $1.29^{0.74}_{-0.47}$ | $1.55^{+0.15}_{-0.16}$ | |
| | (PL) | | $6.69^{+33.31}_{-6.683}$ | $1.73^{+0.75}_{-2.28}$ | 27.8 (free; $^{+25.3}_{-21.9}$) |
| PEAK − Q | BB | 1.77 (42) | $0.60^{+0.04}_{-0.04}$ | $2.75^{+0.05}_{-0.06}$ | 1.9 (free; <8.0) |
| | BB + PL (BB) | 1.55 (40) | $0.61^{+0.10}_{-0.11}$ | $2.66^{+0.15}_{-0.14}$ | |
| | (PL) | | $2.92^{+5.18}_{-2.10}$ | $1.20^{+1.00}_{-0.54}$ | 15.0 (free; <49.0) |
| DECLINE − Q | BB | 1.46 (42) | $1.61^{+0.69}_{-0.42}$ | $1.53^{+0.11}_{-0.10}$ | 65.0 (free; $^{+22.3}_{-20.0}$) |
| | BB + PL (BB) | 1.09 (40) | $2.00^{+3.73}_{-1.94}$ | $1.32^{+0.78}_{-0.52}$ | |
| | (PL) | | $51.4^{+4000.0}_{-50.996}$ | $2.55^{+2.33}_{-2.97}$ | 121.0 (free; $^{+104}_{-64}$) |
| PEAK[a] | BB + PL (BB) | 1.81 (41) | $0.56^{+0.05}_{-0.05}$ | $2.75^{+0.06}_{-0.05}$ | |
| | (PL) | | $13.2^{+7.0}_{-5.2}$ | 1.89 (fixed) | 10.5 (free; $^{+9.7}_{-9.5}$) |
| DECLINE[a] | BB + PL (BB) | 1.64 (41) | $1.21^{+0.25}_{-0.19}$ | $1.56^{+0.08}_{-0.08}$ | |
| | (PL) | | $10.3^{+3.2}_{-3.8}$ | 1.89 (fixed) | 31.7 (free; $^{+10.0}_{-10.0}$) |

[a] No quiescent subtraction.

© American Astronomical Society • Provided by the NASA Astrophysics Data System

1992ApJ...400..330S



better than that to PEAK − D. The residuals to the blackbody fit indicate that an extra component is necessary, similar to that observed in burst 3; however, we can exclude a column in excess of a few $\times 10^{22}$ cm$^{-2}$ with confidence (note that typically $N_H$ is found to be $\sim 7 \times 10^{23}$ cm$^{-2}$ at the deepest part of the dips in both the *EXOSAT* data [Paper I] and the current work [above]).

For the DECLINE bin, the subtraction of the dip spectrum (DECLINE − D) requires the $N_H$ for the blackbody component to be small, whereas subtracting the quiescent spectrum (DECLINE − Q) requires a heavily absorbed blackbody component. Assuming that both components pass through the same absorbing matter, the value of $N_H$ appropriate for this bin appears to be somewhere between the quiescent and dip values.

A consistent explanation for our spectral fitting results is that the burst photoionizes the material which causes the dips. This material then recovers to its normal state during the same 16 s interval as the burst decay.

Fitting the PEAK and DECLINE data without first subtracting a quiescent or dip continuum component gives practically identical conclusions. The power-law photon index is not well constrained in these fits, with possible values ranging from 1.9 to 0.9, but the derived column density is still an order of magnitude too small to be consistent with that measured from the dip spectra. Figure 11 shows the fits to the unsubtracted PEAK and DECLINE spectra; the total flux in the power-law component exceeds the quiescent flux by factors of 2.0 and 1.6, respectively, for the PEAK and DECLINE bins, supporting our interpretation that the ionization of the obscuring material allows us to see the underlying accretion disk component.

We have carefully considered how the low time resolution during the dip may affect these results. Our analysis and simulations of dip data show that a fast modulation in the column density can produce an apparent soft excess during the nonbursting intervals. A similar soft excess may result from the rapid evolution of the burst during the rise, resulting in an apparently low $N_H$ in the fit. However, modeling using the analysis of the burst 3 PEAK − Q spectrum suggests that for the worst case this would increase the $\chi^2_\nu$ to a maximum of $\sim 3$. In contrast, the burst 2 PEAK − D fits are much poorer than this even when low $N_H$ values are used; a model in which a large and constant column ($\sim 2 \times 10^{23}$ cm$^{-2}$) persists from the preburst period until after the DECLINE bin results in a very large $\chi^2_\nu$, in excess of the level which could be accounted for by a rapid change in the spectral shape. We therefore conclude that there was a real decrease in $N_H$ of two orders of magnitude during the dip, caused directly by the burst.

Eighty seconds after the burst, the flux from XB 1916−053 returns temporarily to its quiescent value. Fitting spectra accumulated during this interval, we find results consistent with the normal quiescent spectrum and inconsistent with a blackbody spectrum; therefore, it is clear that this is not a second, less intense burst but a normal quiescent interval.

The integrated intrinsic bolometric fluxes of the bursts are: $5.0 \times 10^{-8}$ ergs cm$^{-2}$ for burst 3; $7.1 \times 10^{-8}$ ergs cm$^{-2}$ for burst 2(Q); $7.4 \times 10^{-8}$ ergs cm$^{-2}$ for burst 2(D). Comparing these with the range of bolometric fluxes observed with *EXOSAT* (Paper I), we can see that burst 2 is ironically one of the more energetic bursts seen in recent observations.

## 5. DISCUSSION

### 5.1. *The Multiple Periodicities in XB 1916−053*

Time-series analysis of the latest *Ginga* observation of XB 1916−053 confirms the results presented in Paper II; we find

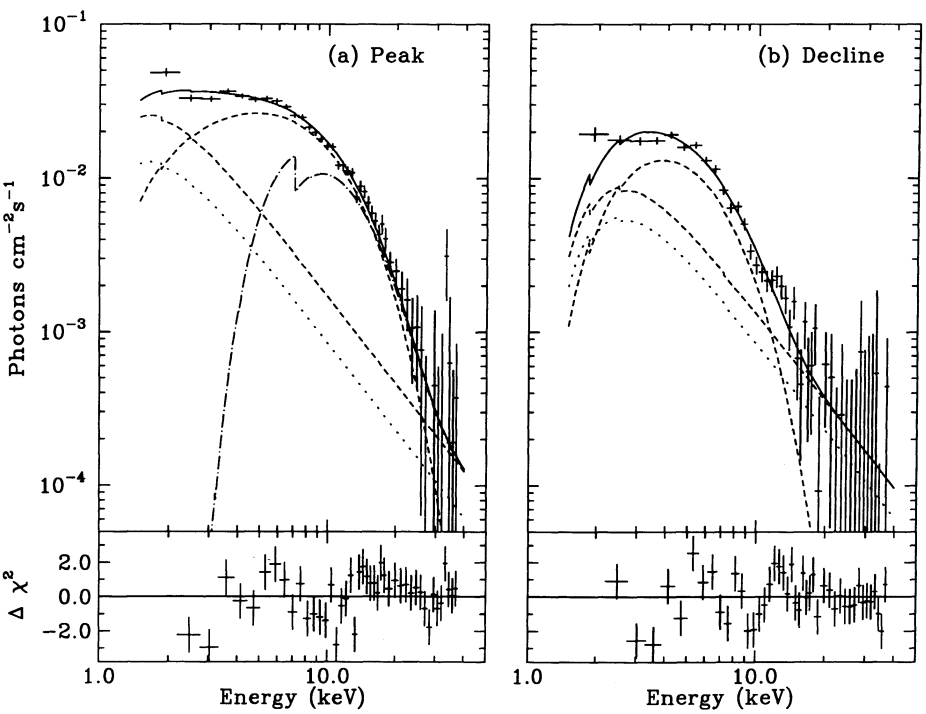


FIG. 11.—As Fig. 10 for burst 2, the burst that occurs during a dipping interval. As before, the dashed lines show the contributions of the individual power-law and blackbody components, and the dotted line, the spectrum of the quiescent emission. In addition, the dot-dash line shows the spectrum that would be observed if the burst emission were absorbed by the column density of $5 \times 10^{23}$ cm$^{-2}$ normally seen during a dip. The data are clearly inconsistent with such an absorption.

© American Astronomical Society • Provided by the NASA Astrophysics Data System

1992ApJ...400..330S



an X-ray primary dip recurrence period for XB 1916−053 consistent with previous X-ray measurements but significantly different from the optical period (Grindlay et al. 1988). In addition, we have seen the secondary dip migrate significantly in X-ray phase by 0.05 in ~30,000 s, with no corresponding movement or jitter in the phase of the primary dip. An even more extreme migration of secondary dips was observed on the fourth day of the 1987 September *Ginga* observation of XB 1916−053 (Paper II), when the center of secondary dipping activity migrated in phase by ~0.25 over six binary cycles. The variability in the phasing of the second dip thus appears to be a general feature of this system, which needs to be borne in mind when one is performing periodicity analyses but which may provide useful constraints on physical models.

Grindlay et al. (1988) and Grindlay (1989) have advanced a model in which XB 1916−053 is a part of a hierarchical triple system. They suggest that the stability of the optical period implies that it is the true orbital period, while the third body in the system causes mass transfer modulation which leads to the X-ray dips having a slightly shorter period. This would mean that the geometry of XB 1916−053 differs substantially from other systems; observationally, the azimuthal structures causing dips and sinusoidal variations in eclipsing systems such as X1822−371, XB 1658−298, and EXO 0748−676 are clearly fixed in the binary frame.

An alternative viewpoint is that the recent, extensive X-ray observations (Paper I, Paper II, and this paper) are similarly consistent with a single, stable primary dip period, and that we should look elsewhere for an explanation of the discrepancy between the optical and X-ray periods.

We note that multiple periodicities are not uncommon among cataclysmic variables (CVs). Using the Ritter (1990) catalog, we find six systems with an apparently stable photometric period ranging from 0.83 to 1.08 times the spectroscopic period, after excluding those systems in which the multiple periodicity is either transient (SU UMa types; see below) or known to be due to the spin period of a magnetic white dwarf. TV Col, for example, has a 5.2 hr photometric period, probably caused by precession of the accretion disk, which is quite distinct from the 5.5 hr spectroscopic period (Barrett, O'Donoghue, & Warren 1988 and references therein). These nonorbital photometric periods in CVs are stable over several years; thus, the observed stability of the optical period of XB 1916−053 is not in itself conclusive evidence for it being the orbital period.

White (1989) considers the possibility that a precessing, elliptical disk exists in XB 1916−053, and that the variation in the projected area of this disk causes the optical modulation. In this model, the disk semimajor axis is required to rotate once every 1.01 orbital periods in the inertial frame. Again, we can consider this hypothesis in the light of recent studies of CVs.

During superoutbursts of the SU UMa subtype of CVs, so-called superhumps or brightness maxima recur at a period $P_s$, which is a few percent longer than the observed orbital period, $P_o$. Numerical simulations predict that an elliptical disk will rotate in the inertial frame with a period of days ($P_p$) (Whitehurst 1988). $P_s$ is believed to be the beat between $P_o$ and $P_p$ on which the tidal stress acting on the elliptical disk, and hence the optical brightness of the disk, is modulated. The Whitehurst model explains all major features of the superoutburst phenomenon (see also Honey et al. 1988 and references therein). However, the optical luminosity of XB 1916−053 is believed to be dominated by the reprocessing of X-rays on the disk. The Whitehurst model predicts that the projected area of the accretion disk will be modulated at $P_p$, not $P_s$ as White (1989) requires. Thus, a purely *geometric* effect is not sufficient to explain the optical behavior of XB 1916−053.

However, the Whitehurst model may be still applicable to XB 1916−053, in the sense that the physical properties of the disk are predicted to vary on $P_s$ due to variable tidal stress. In particular, the disk height is determined by the balance between the vertical component of gravity and the gas pressure (e.g., Ko & Kallman 1991, eq. [7.2]). When the outermost part of the elliptical disk is nearest the secondary, it adds significantly to the vertical component of gravity, which may nearly double depending on the mass ratio and precise location of the disk edge. Thus the disk height will decrease, and so will the irradiation; there should be positive feedback since the decreased irradiation leads to a decreased temperature in the disk (which is presumably radiation-dominated), further decreasing the disk height and leading to decreased optical brightness of the disk. Thus, the *height* of the disk structure and the resulting optical brightness would be modulated on $P_s$ while the *position* of the azimuthal structure would remain fixed, with the X-ray dip period being equal to the orbital period. Thus, our adaptation of the elliptical disk model can explain the observed discrepancy in periods.

Additional evidence for the complicated nature of the emission from XB 1916−053 arises from the study of recent optical observations in which both the original 3027 s optical period *and* the 3000 s X-ray dip period are clearly visible in the cleaned optical power spectrum (Grindlay 1991). In addition, the mean optical light curve is found to change on a time scale of ~4 days, just as the form of the X-ray light curve changes on this time scale (Paper II). Unfortunately, these new observational facts can be fitted into either of the current models for the system; Grindlay (1991) points out that the optical modulation on the X-ray period can originate in reprocessing from the same regions that produce the X-ray dips, while we might equally claim that the presence of a weaker optical modulation on the X-ray period is consistent with our own hypothesis. It seems that only a more extensive campaign of simultaneous X-ray and optical observations can lead to a conclusive solution to the riddle of the multiple periodicities in XB 1916−053.

### 5.2. *Dip Spectra: Data and Simulations*

Turning now to spectroscopy: we have performed spectral analyses of the data from both sources and in addition have successfully modeled the effects of a rapidly changing column density upon the spectral fitting results for XB 1916−053 and EXO 0748−676. This modeling shows that if the dip transition time is shorter than the intensity-selected spectral integration time, the spectral mixing effect is a valid interpretation of the data. The *Ginga* data from XB 1916−053 have been studied down to a time resolution of 4 s (this paper), and the *EXOSAT* data to a resolution of 2 s (Paper I); for EXO 0748−676 the *EXOSAT* data have been studied to a resolution of 1000 s (Parmar et al. 1986) and the *Ginga* data to 16 s (this paper). In all of these cases a two-component model is required to fit the dip data. Thus, if this effect is responsible, the time scale for variability in the depth of the absorbing material in the line of sight must be $<2$ s for XB 1916−053 and $<16$ s for EXO 0748−676.

We assume that in each source the accretion disk fills a large fraction of its Roche lobe. In XB 1916−053 the disk edge is at

© American Astronomical Society • Provided by the NASA Astrophysics Data System

1992ApJ...400..330S



a distance from the central source of $2.3 \times 10^{10}$ cm. If the accretion disk structure is at this distance, the Keplerian velocity is $9 \times 10^7$ cm s$^{-1}$, giving a length scale for the clumpiness of the material of $< 1.8 \times 10^8$ cm. For EXO 0748−676 with an accretion disk size of $5.0 \times 10^{10}$ cm, the Keplerian velocity is $6.1 \times 10^7$ cm s$^{-1}$ and the length scale is $< 9.8 \times 10^8$ cm. These are rather conservative upper limits, as an examination of dip transitions for EXO 0748−676 shows that variability can occur down to a time scale of a few seconds (Parmar et al. 1986).

There are other sources for which the column density changes rapidly, and it may be worthwhile to investigate whether spectral mixing is important in these cases. One example is the absorption spectrum of the high-mass X-ray binary pulsar Vela X-1. Observations performed using *Tenma* (Nagase et al. 1986) and *EXOSAT* (Haberl & White 1990) reveal an absorption spectrum with a soft excess over that expected from simple photoelectric absorption. The authors of both these papers put forward complex physical models for the source behavior but do not consider the spectral mixing effect even though the column density changes on a similar time scale to the spectral integration times used. The magnitude of the effect should be considered in further physical modeling of this and other systems.

### 5.3. *A Brightening of the Disk Component during Bursts?*

Analysis of the X-ray burst data from XB 1916−053 suggests that the bursts may have a significant impact on the emission observed from the disk. Spectral fits to our burst 3 show that the continuum emission from the disk appears to increase significantly by a factor of up to 3 as a result of the burst, perhaps caused by increased Comptonization by the incident photon flux from the burst.

We note that excesses below 3 keV and above 15 keV similar to those described here were also seen in the burst spectra of XB 1916−053 obtained by the *HEAO 1* A-2 (Swank, Taam, & White 1984). Studies of bursts from other objects, e.g., X1608−52 (Nakamura et al. 1989), also provide examples of burst spectra in which a clear excess over a simple blackbody is observed above 10 keV. Comptonization of the blackbody (Nishimura, Mitsuda, & Itoh 1986) or a small reflection component from the disk (Day & Done 1991) are also viable explanations for a high-energy tail but do not explain a lower-energy excess. XB 1916−053 has a somewhat lower column than many other Galactic center binaries, perhaps making low-energy effects easier to detect in this source. With improved time resolution, the peak burst emission will exceed the disk emission by a much greater factor and may swamp the increase in the disk component. Of course, since the burst fluence changes so rapidly on a short time scale, the disk spectrum must also react to the changes, and any spectral fit will be a time-average.

### 5.4. *Ionization of Azimuthal Material during Bursts*

In addition, our results indicate that the burst which occurs during a dip episode ionizes almost all of the obscuring medium in the azimuthal structure, which then relaxes back to its cooler state on a time scale similar to that of the burst. For this to be feasible, two conditions have to be satisfied: first, the observed time scales have to be consistent with theoretical ionization and recombination time scales, and second, the number of extra photons emitted during the burst must be considerably larger than the total number of atoms that are to be ionized.

For a cloud (or blob) with time scale size $l$ at a distance $R$ from a source of luminosity $L$, the ionization time scale $t_{\rm ion}$ is equivalent to the inverse of $L\sigma/4\pi R^2\epsilon$, where $\epsilon$ is the mean X-ray energy and $\sigma$ is the photoionization cross section. Thus,

$$t_{\rm ion} \sim 10^{-6} L_{38}^{-1} R_{10}^2 \sigma_{-20}^{-1} \epsilon_{-9} \text{ s} ,$$

where $L_{38}$, $R_{10}$, $\sigma_{-20}$, and $\epsilon_{-9}$ are in units of $10^{38}$ ergs cm$^{-2}$ s$^{-1}$, $10^{10}$ cm, $10^{-20}$ cm$^2$, and $10^{-9}$ ergs, respectively.

The recombination time scale $t_{\rm rec}$ is similarly the inverse of the product of the gas density $n$ and the recombination rate as a function of temperature $\alpha(T)$. From Allen (1973), $\alpha = 2 \times 10^{-11} Z^2 T^{-1/2}$ and thus is of order $10^{-13}$ cm$^3$ s$^{-1}$ for a temperature of $10^4$ K. So, since the column density $N_{\rm H}$ is given by $N_{\rm H} = nl = 10^{23} l_8 n_{15}$,

$$t_{\rm rec} \sim 10^{-2} n_{15}^{-1} \alpha_{-13}^{-1} \text{ s} .$$

When a burst occurs $L$ increases quickly and $t_{\rm ion}$ drops, leading to a rapid increase in ionization. As $L$ decays back to its quiescent level, the ionization time scale increases again and the material recombines and becomes increasingly opaque to low-energy photons. These large changes in ionization structure can occur over time intervals $< 1$ s.

The number of photons emitted by the burst and available at the radius of the obscuring material is given by

$$N_{\rm phot} = \frac{L \Delta t}{\bar{\epsilon} 4\pi R^2}$$

per unit area, where $\bar{\epsilon}$ is the mean X-ray energy and $\Delta t$ is the duration of the most luminous portion of the burst event. For $L \gtrsim 10^{38}$ ergs s$^{-1}$, $\bar{\epsilon} \sim 1$ keV, and $\Delta t \sim 1$ s, $N_{\rm phot} \sim 10^{26}$ cm$^{-2}$. This is several orders of magnitude greater than the column density.

To summarize, we propose that this energetic burst ionized the obscuring medium in the line of sight, which then relaxed back to equilibrium on a time scale similar to that of the burst decay. The time scales and fluxes involved support this hypothesis. However, in order to confirm this suggestion and study the phenomenon in greater detail, more bursts in dips need to be observed and analyzed, preferably using a higher time resolution. Such observations would not only confirm if the $N_{\rm H}$ change is real but also check against the rather unlikely possibility that a physically unrelated change in the dip depth occurred at the time of the burst by pure chance. It is also desirable to observe such an event with a higher sensitivity below 2 keV than that of the *Ginga* LAC; at lower energies, we would expect to see the effects of the burst on the lighter elements in the absorbing medium.

We acknowledge the facilities of the X-Ray Astronomy Group, Physics Department, University of Leicester, and the Mullard Space Science Laboratory of University College London, where we performed much of the original spectral analysis for both sources, and the Institute of Space and Astronautical Science in Japan, where we first extracted the data from EXO 0748−676. We are grateful to Tim Kallman and an anonymous referee for helpful comments. K. M. acknowledges the financial support of NASA through contract NAS5-30180, administered by the Space Sciences Laboratory. R. H. D. C. acknowledges the financial support of NASA through contract NAG8-186.

© American Astronomical Society • Provided by the NASA Astrophysics Data System

1992ApJ...400..330S



REFERENCES

Allen, C. W. 1973, Astrophysical Quantities (3d ed.; London: Athlone)
Barrett, P., O'Donoghue, D., & Warner, B. 1988, MNRAS, 233, 759
Day, C. S. R., & Done, C. MNRAS, 253, 35P
Frank, J., King, A. R., & Lasota, J.-P. 1987, A&A, 178, 137
Gottwald, M., Haberl, F., Parmar, A. N., & White, N. E. 1986, ApJ, 308, 213
Grindlay, J. E. 1989, in Proc. of the 23rd ESLAB Symposium (ESA SP-296), (Noordwijk: ESA), 121
———. 1991, in Proc. of the 28th Yamada Conference; Frontiers of X-ray Astronomy, ed. Y. Tanaka & K. Koyama (Tokyo), 69
Grindlay, J. E., Bailyn, C. D., Cohn, H., Lugger, P. M., Thorstensen, J. R., & Wegner, G. 1988, ApJ, 334, L25
Haberl, F., & White, N. E. 1990, ApJ, 361, 225
Hayashida, K., et al. 1989, PASJ, 41, 373
Hellier, C., & Mason, K. O. 1989, MNRAS, 239, 715
Hirose, M., Osaki, Y., & Mineshige, S. 1991, PASJ, 43, 809
Honey, W. B., Charles, P. A., Whitehurst, R., Barrett, P. E., & Smale, A. P. 1988, MNRAS, 231, 1
Ko, Y.-K., & Kallman, T. 1991, ApJ, 374, 721
Lubow, S. H. 1989, ApJ, 340, 1064
Mason, K. O., & Córdova, F. A. 1982, ApJ, 262, 253
Nagase, F., Hayakawa, S., Sato, N., Masai, K., & Inoue, H. 1986, PASJ, 38, 547
Nakamura, N., Dotani, T., Inoue, H., Mitsuda, K., Tanaka, Y., & Matsuoka, M. 1989, PASJ, 41, 617
Nelson, L. A., Rappaport, S. A., & Joss, P. C. 1986, ApJ, 304, 231
Nishimura, J., Mitsuda, K., & Itoh, M. PASJ, 38, 819
Parmar, A. N., Smale, A. P., Verbunt, F., & Corbet, R. H. D. 1991, ApJ, 366, 253
Parmar, A. N., White, N. E., Giommi, P., & Gottwald, M. 1986, ApJ, 308, 199
Ritter, H. 1990, A&AS, 85, 1179
Smale, A. P., Mason, K. O., White, N. E., & Gottwald, M. 1988, MNRAS, 232, 647 (Paper I)
Smale, A. P., Mason, K. O., Williams, O. R., & Watson, M. G. 1989, PASJ, 41, 607 (Paper II)
Swank, J. H., Taam, R. E., & White, N. E. 1984, ApJ, 277, 274
Turner, M. J. L., et al. 1989, PASJ, 41, 345
White, N. E. 1989, A&A Rev, 1, 85
White, N. E., & Holt, S. S. 1982, ApJ, 257, 318
White, N. E., & Swank, J. H. 1982, ApJ, 253, L61
Whitehurst, R. 1988, MNRAS, 232, 35

© American Astronomical Society • Provided by the NASA Astrophysics Data System